

# Soft Lithography for Manufacturing Scalable Perovskite Metasurfaces with Enhanced Emission and Absorption

Amit Kessel, Christian Frydendahl, Sita Rama Krishna Chaitanya Indukuri, Noa Mazurski, Pankaj Arora, and Uriel Levy\*

Organic–inorganic hybrid perovskites have emerged in recent years as a promising alternative to silicon solar cells and other optoelectronic devices, mostly due to their high photon yields, long carrier lifetime, adjustable bandgap, and other merits. While patterning photonic nanostructures onto their inorganic counterparts is well established to augment their capabilities, lack of compatibility with conventional lithography techniques hinders the implementation of those principles with perovskites. Hereby, the fabrication of MAPbI<sub>3</sub> nanophotonic structures such as nanoscale metasurfaces is demonstrated via soft lithography, a method in which the patterning is done when the perovskite is not fully crystallized, allowing for crystallization within the mold with the end result of facile and unarmful imprinting of sub-micron features onto perovskite thin films, over large areas and with the potential to scale up in a seamless way. By doing so, a substantial increase in light absorption as well as twofold photoluminescence enhancement from the perovskite thin film is shown. These results are supported by spectral and lifetime measurements. This method is pertinent to many device configurations and can assist in realizing the future of high-efficiency perovskite-based devices, including solar cells, LEDs, lasers, and more.

Over the last decade, organic–inorganic hybrid perovskites have been extensively researched due to their extraordinary properties allowing for low cost, high efficiency, and solution processed solar cells and other optoelectronic devices. By patterning the perovskite film into a nanoscale photonic structure such as a metasurface, its optical properties can be further enhanced or manifested to achieve a myriad of applications.<sup>[1,2]</sup> Surface texturing for improved sunlight harvesting has long ago evolved in nature, as some tropical plants residing in low light conditions grow surface textured leaves which focuses light into their photosystem more efficiently.<sup>[3–6]</sup> While silicon solar cells are produced with patterned surfaces to achieve better light manage-


ment and higher efficiencies, applying the same principles with perovskites is challenging. Unfortunately, conventional patterning techniques, commonly used with inorganic semiconductors, are less appropriate for hybrid perovskites. Direct writing of nanoscale features on a perovskite film was demonstrated through ultrafast laser patterning.<sup>[7]</sup> Electron-beam lithography has been used as well,<sup>[8,9]</sup> yet this process typically results in isolated structures rather than continuous patterned films. Moreover, most of the commercial photoresists will cause the perovskite to chemically degrade. A careful selection of materials for each step has been shown to achieve isolated micro-structures.<sup>[10]</sup> Several alternative methods have been suggested such as wet-ability-assisted lithography.<sup>[11]</sup> Hörantner et al. demonstrated template assisted patterning through colloidal lithography, which showed enhanced efficiency of solar cells.<sup>[12]</sup> While in principle it can be scaled over large areas, this method is limited to a

single pattern and requires additional fabrication steps. On the other hand, nanoimprint lithography (NIL) is regarded with high potential to produce perovskite metasurfaces. By pressing a hard stamp on a heated film, a chemically dry process of large area imprinting can be achieved. Nanoimprinted perovskite metasurfaces have shown substantial emission enhancement,<sup>[13]</sup> distributed feedback lasing,<sup>[14]</sup> and photodetectors with improved efficiency.<sup>[15]</sup> However, NIL is usually applied with polymers, where they are brought above their glass transition temperature in order to induce the fluidity required for reshaping. Since hybrid perovskites are crystalline materials with no glass transition temperature, and overheating initiates degradation, temperatures must be kept relatively low (around 100 °C). Thus, tremendous pressures must be exerted which requires complex and expensive machinery on one hand, and may also place a stringent limitation on the durability of such devices on the other hand as unnecessary exposure to the environment happens during the transfer of the film to the NIL machine. Moreover, applying such high pressure requires the use of a rigid silicon stamp. Fabricating it with sub-micron features, especially over large areas is expensive and time consuming. Silicon stamps tend to become damaged after multiple imprints which hinders the producibility of such patterned samples.<sup>[16]</sup>

In this paper, we demonstrate scalable patterning of MAPbI<sub>3</sub> metasurfaces through soft lithography, specifically Soft Molding

A. Kessel, Dr. C. Frydendahl, Dr. S. R. K. C. Indukuri, Dr. N. Mazurski, Prof. P. Arora, Prof. U. Levy  
Department of Applied Physics  
Faculty of Science and the Center for Nanoscience and Nanotechnology  
The Hebrew University of Jerusalem  
Jerusalem 9190401, Israel  
E-mail: ulevy@mail.huji.ac.il

Prof. P. Arora  
Birla Institute of Technology and Science  
Pilani, Rajasthan 333031, India

 The ORCID identification number(s) for the author(s) of this article can be found under <https://doi.org/10.1002/adom.202001627>.

DOI: 10.1002/adom.202001627

(SOMO), as well as considerations for achieving a successful pattern transfer. Through that, we study the effects of imprinting perovskite nanophotonic structures on their optical properties and explain the physical mechanisms which lead to an enhanced absorption and emission. We conclude by discussing the implications of implementing such structures in optoelectronic devices on their performance.

Soft lithography is a family of techniques which utilize soft elastomeric stamps to transfer the pattern onto the material.<sup>[17]</sup> That way, a conformal contact can be kept with flexible substrates and viscous materials. Unlike NIL, the patterning is done when the perovskite is in solution form, allowing for crystallization within the mold and therefore only a mild pressure is needed. Together with an easy reproducibility of the stamp, it makes soft lithography the preferred alternative. This method is being used to enhance the performance of organic solar cells<sup>[18]</sup> and a few studies have employed it to perovskites as well.<sup>[19,20]</sup> Jeong et al. fabricated a variety of perovskite micropatterns,<sup>[21]</sup> Chun et al. demonstrated a nanopillar photodetector with enhanced photoresponse<sup>[22]</sup> and a compact disc grating pattern was used to achieve more efficient and stable solar cells.<sup>[23,24]</sup> The process of SOMO is depicted in **Figure 1a**. Generally, the solution is deposited on the substrate to form a not yet crystallized, viscous thin film. Next, an elastomeric mold is pressed on the film, using a custom-made press unit (Figure S1, Supporting Information), and they are heated together to allow for solvent evaporation and crystallization of the material within the mold. Finally, the mold is detached and a patterned film is achieved.

For the stamp material, we used polydimethylsiloxane (PDMS), which is widely used in soft lithography and can be easily reproduced from a silicon master mold. In that case, a high Young's modulus PDMS (hPDMS) is necessary to successfully replicate nanoscale high aspect ratio features<sup>[25,26]</sup> and to prevent deformations under the applied pressure (Figure S2, Supporting Information).

Due to the variety of hybrid perovskite compounds and deposition techniques being used, understanding of the imprint process can be helpful when trying to apply it for different experimental conditions. As illustrated in Figure 1b, several forces come into play. The perovskite is driven into the gaps of the mold by the external pressure and by capillary rise. According to Jurin's law,<sup>[27]</sup> the capillary rise into a tube channel is inversely proportional to its radius and therefore will become dominant for smaller features. During the rise, the solvent evaporates and is absorbed in the mold. A rule of thumb is that in order to get a complete filling of the gap, the rate of solvent absorption must be greater than the rate of evaporation. This prevents accumulation of vapors and a corresponding resistive pressure in the gap between the rising perovskite and the mold.<sup>[28]</sup> While the solvent absorption rate is a constant which is determined by the stamp's material, the rate of evaporation can be controlled through the selection of solvent<sup>[29]</sup> and annealing temperature. At higher temperatures, solvents evaporate more rapidly. Overheating may lead to untimely crystallization, before completely filling the mold. We find that for MAPbI<sub>3</sub>, standard annealing temperatures (90–100 °C) are sufficient for that manner.

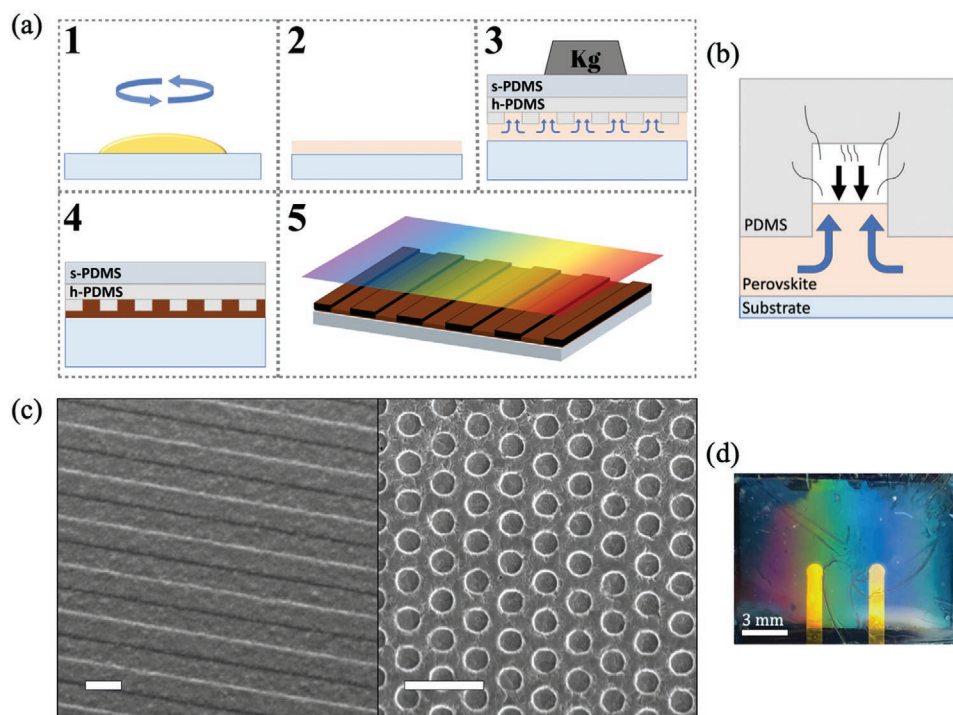


**Figure 1.** a) SOMO schematic process. 1) Perovskite is deposited to form a 2) semi viscous thin film. 3) An elastomeric stamp is pressed onto the film which in response fills the voids within the features, 4) annealing to remove solvent and crystallization, 5) a structured perovskite film is created. b) Mold filling process. The perovskite fills the mold due to the external pressure and/or capillary rise. In the process, the solvents are evaporated and absorbed into the mold. When the rate of absorption is smaller than for evaporation, then a resistive vapor pressure is present in the gap between the rising perovskite and the mold. c) SEM images of MAPbI<sub>3</sub> films patterned (left—1D patterning, right—2D patterning) through SOMO. Scale bar is 1 μm. d) A large area imprint with the grating pattern in (c), demonstrating a large area iridescent surface.

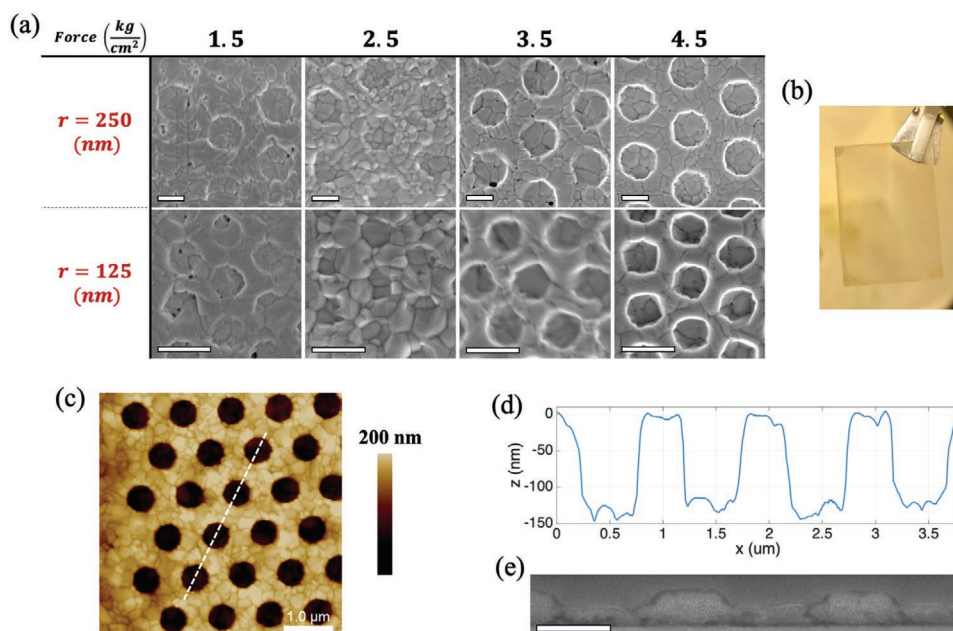


**Figure 2.** a) SEM micrograph of imprint comparisons for varying pressing forces, for  $r = 125$  and  $250$  nm. A force of about  $4 \text{ kg cm}^{-2}$  is needed for a successful transfer of the pattern. Scale bar  $500 \text{ nm}$ . b)  $\text{MAPbI}_3$  film as-deposited, prior to the imprint. A transparent phase indicates that the film is not crystallized and can flow into the mold. c) AFM image of  $500 \text{ nm}$  diameter hole array and d) cross section profile from the white dotted line. e) FIB cross section, showing slightly cone-shaped holes. Scale bar  $500 \text{ nm}$ .

Figure 1c presents  $\text{MAPbI}_3$  films imprinted with 1D and 2D patterns through SOMO and Figure 1d shows an image of the diffraction grating structure in Figure 1c, demonstrating that a large area, iridescent surface can be achieved.

To investigate the effect of patterning a perovskite film, we imprinted hexagonally shaped, nano-hole arrays (as in Figure 1c) with diameters ranging from  $250$  to  $500 \text{ nm}$ .

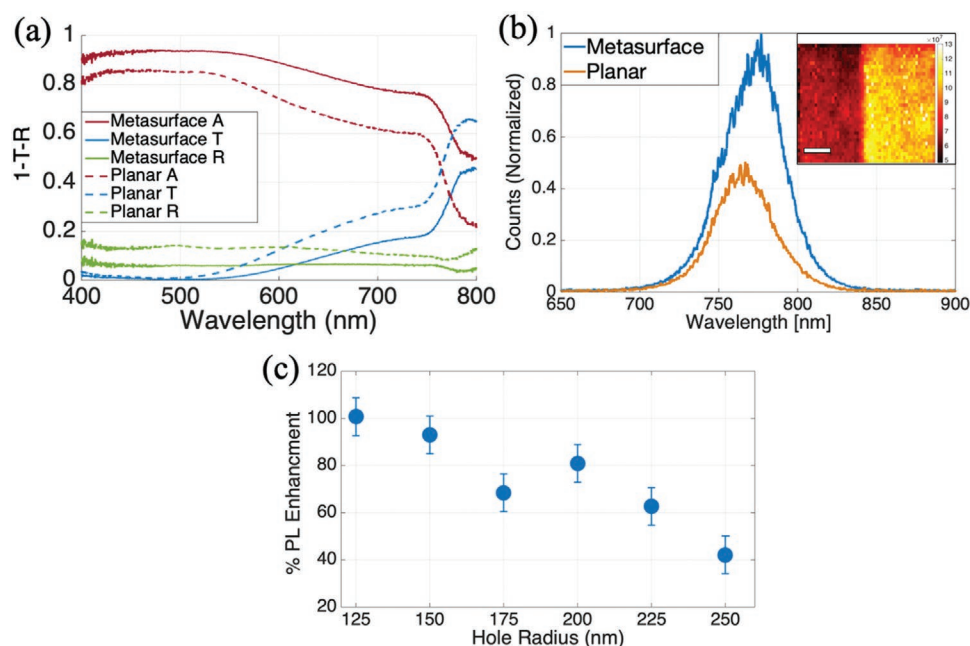
A circular structure reduces polarization and angle dependency and is therefore suitable for solar applications. By comparing the imprint from various pressing forces (Figure 2a), we can see that the force is a dominant factor for determining the quality of the imprint. For both the largest and the smallest array we observe that a force of about  $4 \text{ kg cm}^{-2}$  (pressure of  $\approx 4$  bar) is needed for a complete transfer of the pattern. We observed that further increasing the force does not improve the quality of the imprint. Of course, there is an interplay between the exerted force and the film's viscosity. The more solvents evaporate, the more force the less-fluidic perovskite requires in order to drive it into filling the mold and vice versa. Thus, a complementary image of the as-deposited  $\text{MAPbI}_3$  film prior to the imprint is shown in Figure 2b. An almost completely transparent phase indicates that crystallization has hardly begun, making the film susceptible to patterning. The as-deposited film's viscosity can be adjusted by several parameters such as solvent selection, solution concentration, anti-solvent amount (often used to prepare high quality films<sup>[30]</sup>), and spin coating speed. A detailed analysis on solvent selection for perovskite soft lithography was done by Britzman et al.<sup>[29]</sup> To further characterize the imprinted structure, an atomic force microscopy (AFM) measurement was taken, along with a cross section image obtained by focused ion beam (FIB) milling. The results for the  $500 \text{ nm}$  diameter hole array are presented in

Figure 2c,d,e. A uniform array of nano-holes is achieved with a mean diameter of  $545 \pm 17 \text{ nm}$  and a depth of  $127 \pm 14 \text{ nm}$ , which is a little less than the depth of the silicon master mold ( $\approx 148 \pm 2 \text{ nm}$ ). From Figure 2d,e, we observe a slightly cone shaped structure which may happen due to an incomplete cover of the PDMS mold by the perovskite. For the planar region, the roughness has a root mean square value of  $11.8 \text{ nm}$ . It also shows that a relatively planar film is achieved outside of the patterned area. This indicates that the very act of pressing flat PDMS on top of the perovskite film during crystallization can assist in creating a flat, densely packed, and high quality film.

Next, optical characterizations were performed. For each of the arrays, reflection and transmission spectra were taken across the visible regime, with comparison to the planar region on the film. Figure 3a presents the measurement (solid line) for the  $500 \text{ nm}$  diameter hole array (other diameters show same qualitative behavior) compared to a planar film, averaged over several locations (dashed line). While the material is very much absorptive to begin with, we observe a further enhancement in absorption. Clearly, absorption enhancement will become more dominant for a thinner film device, having a lower initial absorption. A clear resonance cannot be seen since the material is very lossy, that is, the relatively high absorption dampens and broadens any resonant peak which may arise. Significant resonances of the structure are expected to be observed in the infrared regime, where the photon energies are below the band gap energy of the material, and the structure thus stops being absorbing.

As shown, reflection reduces quite uniformly along the spectrum, which implies random surface scattering is taking a role, by directing light into the perovskite with part of it going to wide angles, larger than the numerical aperture of the light





**Figure 3.** a) Absorption (A), transmission (T), and reflection (R) comparison between nano-hole metasurfaces (solid line) and a planar film (dashed line). b) PL spectra of the  $r = 125$  nm array versus a planar surface. Inset shows a PL map of the border between the metasurface (bright yellow) and the planar (dark red) regions. Scale bar  $10 \mu\text{m}$ . Excitation wavelength is  $514 \text{ nm}$  c) External emission enhancement for every hole size. Error bars were estimated experimentally.

collecting objective. Therefore, we should note that the actual absorption is likely to be slightly less than what is directly derived from the measurement. Transmission is also reduced for wavelengths longer than  $500 \text{ nm}$ , where it is not negligible to begin with. This can be attributed to a longer optical path in the perovskite and coupling to waveguide modes. An FDTD simulation of the electric field, confirms the waveguide modes arising in the nano-hole perovskite layer as well as a localization of the field inside the cavity (Figure S3, Supporting Information). We observe that for longer wavelengths (relative to the cavity's size), the field is less localized in the cavity and leaks into the perovskite where it is being guided and absorbed. This observation further supports the reduction in transmission, which increases for longer wavelengths. Absorption is calculated as  $A = 1 - T - R$ . In order to assess the contribution for generating free carriers under solar illumination, we calculated the portion of photons to be absorbed under AM1.5 illumination, in the range of  $400\text{--}800 \text{ nm}$ . This was done by multiplying the absorption spectra with the irradiance from the Sun. For the planar film, we obtained an absorption of 69% of the photons whereas for the metasurfaces a value of 83% was found. This corresponds to an overall 20% increase in the number of absorbed photons, which in ideal conditions can enhance the generated electrical current in the cell by a similar amount.

Photoluminescence (PL) was taken from each array, with comparison to the planar region next to it. All of the arrays show enhanced emission. The spectrum of the smallest array ( $r = 125 \text{ nm}$ ) is presented in Figure 3b. We observe a twofold increase in the total external emission, relative to the planar film (by dividing the area below the two lines), along with a small red shift, which is likely due to the effectively thinner film, absorbing less of the low energy photons. The inset in Figure 3b

shows a PL map of the border between the metasurface and the planar regions, which emphasizes the phenomenon over larger areas. When comparing the overall enhancement between the arrays we notice a trend where the smaller the hole's size, the larger the emission enhancement (Figure 3c).

To better understand the origin of the large PL enhancement, we consider three possible paths. First, increased absorption will obviously contribute to the external luminescence efficiency. However, we observe a mere  $\approx 15\%$  increase in absorption at the wavelength of excitation ( $514 \text{ nm}$ ), which does not account for the 100% increase in emission.

Second, we consider the modified spontaneous emission arising from the photonic structure (for resonant systems, the Purcell enhancement<sup>[31]</sup>). The emission rate of an emitter is dependent on the surrounding electromagnetic field and local photonic density of states.<sup>[32]</sup> Therefore, a stronger field confinement in the perovskite (Figure S3, Supporting Information) enhances the rate of emission. To verify it experimentally we performed a time resolved photoluminescence (TRPL) measurement. The results for the array with the highest emission are presented in Figure 4a. The average recombination lifetime for the metasurface and the planar were  $7.9$  and  $9.2 \text{ ns}$  respectively. While those are relatively small values for this material, we are interested in the relative change, which is  $\approx 15\%$ . The high optical damping, along with an imperfect cylindrical hole,<sup>[33]</sup> hinder the intensification of the field inside the perovskite. Thus, the contribution of this phenomenon to the external emission enhancement is not large. Altogether, we reach about 32% increase which is yet insufficient to describe the entire enhancement we see.

The third and perhaps the most dominant path is the improved photon outcoupling from the film. It has been already

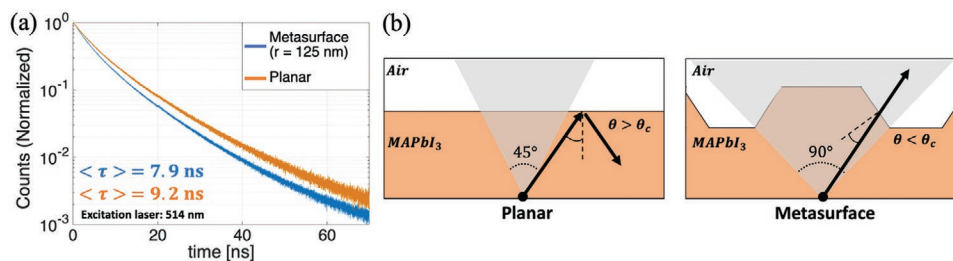


**Figure 4.** a) TRPL measurement for the highest emitting array ( $r = 125 \text{ nm}$ ) compared to the planar region next to it. Average lifetime for the metasurface and planar is 7.9 and 9.2 ns respectively. b) Schematic illustration of the escape cone for a photon emitted inside the perovskite. It represents the range of emission angles which are smaller than the critical angle for total internal reflection,  $\theta_c$ . The structured surface effectively decreases the angle of incidence with the surface and creates greater outcoupling efficiency. For a point emitter at the depicted position, the planar film's cone is  $45^\circ$  wide and for the metasurface, it is  $90^\circ$ , which increases the escape probability by a factor 2.

established that photon recycling (PR), the reabsorption of emitted photons, plays a crucial role in halide perovskites.<sup>[34]</sup> It is mainly observed through the relatively low measured external emission yield in planar films, compared with the expected high internal yield of the material. This means that not all emitted photons are exiting the film and collected at the detector. For MAPbI<sub>3</sub>, the refractive index at the emission peak is 2.6, leading to a total internal reflection critical angle of about  $23^\circ$  at the perovskite-air interface (from which PL was collected in this study). Considering a planar film, an escape cone of about  $45^\circ$  ( $2 \cdot 23^\circ$ ) exists. Under the assumption of an isotropic emission inside the perovskite, it leads to an escape probability of 12.5%, that is, one out of eight photons will be emitted to the environment. Applying an encapsulation layer with refractive index higher than 1 shall improve the light outcoupling as well due to reduced Fresnel reflections. This concept is illustrated in Figure 4b. When creating a textured surface, the angle of incidence relative to the surface normal effectively decreases. This allows more photons to be outcoupled from the system. In that manner, a cone-shaped hole is actually more efficient than sharp cylindrical holes (easily seen through ray optics). The change in escape probability varies spatially inside the perovskite and can grow up to twice as much as for the planar film, for a given angle of emission (as depicted in Figure 4b). We therefore deduce that improved photon outcoupling is responsible for the remaining boost in PL. Recalling an overall increase of 100%, we believe that this mechanism accounts for an increase of about 50% ( $1.15 \times 1.15 \times 1.5 \cong 200\%$ ) in externally emitted photons.

In general, PL enhancement,  $\eta$ , from a patterned film should be regarded as a combination of the aforementioned factors, in a way that  $\eta = a^E(\lambda_0) \int \Gamma^E(\lambda) \eta_{\text{esc}}^E(\lambda) d\lambda$ . Using the relative values for  $a^E(\lambda_0)$  absorption for the wavelength of excitation ( $\lambda_0$ ),  $\Gamma^E(\lambda)$  the spontaneous emission rate and  $\eta_{\text{esc}}^E(\lambda)$  the escape probability (superscript E stands for enhancement). Integration is performed over the entire emission spectrum.

Implementing a patterned perovskite layer is obviously beneficial for light emitting applications. Excluding excitation light absorption, we assess that even for electroluminescence, the external emission efficiency could increase by  $\approx 70\%$ . For solar cells, we need to consider the effect on both the current and the voltage in the cell. In an ideal case, any extra photon absorbed generates a free carrier and as a result an increased current. In addition, features which are deeper than the thickness of the charge transfer layer (CTL) on top serve as a

template for a patterned CTL and electrode as well. By that, its surface area increases, which could create better charge collection efficiency.<sup>[35,36]</sup> Under the detailed balance principle, in ideal conditions, the voltage buildup in the cell is proportional to the incoming light flux.<sup>[37]</sup> Therefore, any process that removes available energy from the system such as photon outcoupling or parasitic absorption, diminishes the voltage from its optimum. At open circuit, efficient external luminescence is an indicator of low internal losses.<sup>[38,39]</sup> Kirchartz et al. have derived that the voltage boost for PSC due to PR could be larger for planar devices over a randomly textured surface by as much as  $\approx 40 \text{ meV}$ .<sup>[40]</sup> Yet a recent paper has analyzed that for a nanophotonic perovskite layer, similar to the one in this study, the voltage boost lays somewhere between the PR efficient planar film and the “inefficient” random texturing.<sup>[41]</sup> This is because part of the emitted photons are coupled to waveguide modes (as previously discussed) and remain in the system. Thus, a nanophotonic perovskite device can benefit from PR without compromising the typical increased absorption in textured films. Further work is needed to clarify this issue.

To summarize, we have demonstrated and examined the process of patterning MAPbI<sub>3</sub> thin films through soft lithography. By harnessing the solution processed nature of this material, embedding nanophotonic structures can be readily done with a home-made pressing machine, making it realizable for non-specialist research groups to examine the effects on their own devices. Such a technique can potentially be scaled up to large areas by seamless integration in the fabrication process. We have shown that a perovskite metasurface can absorb  $\approx 20\%$  more photons under solar illumination due to scattering and coupling to guided modes which enhances the field inside the material. Together with lifetime shortening and increasing the outcoupling by 50%, twofold external emission efficiency is achieved. These merits could be further enhanced through optimization of the nanophotonic structures' design. When tremendous efforts are being put in achieving record efficiencies,<sup>[42]</sup> we believe that combining this method would bring an extra boost in the pursuit towards the Shockley-Queisser limit.

## Experimental Section

**Master Mold:** A silicon  $20 \times 20 \text{ mm}$  chip was cleaned with “Piranha” ( $\text{H}_2\text{SO}_4:\text{H}_2\text{O}_2$  3:1). The pattern was defined by spin-coating of an electron beam resist (ZEP 520A) followed by electron beam lithography

(ELS-G100 Elionix). The pattern was transferred to silicon by reactive ion etching (Corial 2001) with a mixture of SF<sub>6</sub> and CHF<sub>3</sub>. After etching, the remaining ZEP was stripped and the sample was cleaned with "Piranha". Immediately afterwards, an anti-adhesive treatment of octadecyltrichlorosilane (OTS, Sigma Aldrich) was performed through vapor deposition. PDMS stamp: hPDMS (Gelest) base and curing agent were mixed in a 1:1 ratio. 20 wt% of toluene was added to reduce the viscosity and improve the filling of the master mold.<sup>[43]</sup> The mixture was degassed and spin coated on the Si master for 30 s at 2000 RPM to form a thin film and then degassed again, followed by a partial curing for 30 min in the oven at 65 °C until it is slightly sticky. Back layer of soft PDMS (Sylgard 184, Dow) for easier handling of the stamp was prepared by mixing base and curing agents in a 5:1 ratio, degassed, cast on top of the hPDMS followed by a second degassing and placed in the oven overnight for the complete curing. Finally, the double layer PDMS mold is gently peeled from the master.

**Imprint Process:** To prevent interactions with air and moisture during the crystallization of the perovskite, the following is performed inside a nitrogen-filled glovebox. MAPbI<sub>3</sub> solution was prepared by dissolving 1 M of MAI (Ossila) and PbI<sub>2</sub> in DMF:DMSO, with ratio of 4:1 between the solvents (Sigma Aldrich). The solution was kept at 60 °C while stirring for 5 h. Perovskite precursor was spin coated on a pre-cleaned ITO coated glass (Ossila) at 1000 RPM for 10 s followed by 3000 rpm for 20 s. 10–20 μL of toluene was added 15 s after the beginning of the spinning.<sup>[44]</sup> The PDMS mold was pressed with a weight of 4.5 kg cm<sup>-2</sup> using weights on the as-coated film, and they were annealed at 90 °C for 10 min. Finally, the mold is gently removed from the patterned perovskite film which is placed back on the hotplate for the complete removal of residue solvents.

**Absorption Measurement:** Transmission and reflection spectra were measured using a custom microscope setup. For transmission, the sample was illuminated with a white light source (tungsten-halogen lamp) through a microscope condenser lens.<sup>[45]</sup> The transmitted light is collected by an objective lens (Nikon, 50×, NA 0.45) and taken to a fiber coupled Ocean Optics Flame spectroscopy. Reflection measurements were done in an inverted reflection microscope configuration, using the same light source, objective lens, and spectrometer.

**PL Measurement:** Both steady-state and time-resolved measurements were performed using an inverted microscope in reflection mode. The sample is excited using a supercontinuum laser (rep. rate 80 MHz) filtered to a spectral width of ≈4 nm around a central wavelength of 514 nm. PL emission is separated by a dichroic mirror and a long-pass filter, both with cutoff wavelengths of 550 nm. The PL signal was coupled to a fiber that is connected to either the spectrograph (in the case of steady-state measurements) or to a single photon detector (SPAD, for time-resolved measurement).<sup>[46]</sup>

**Numerical Simulations:** FDTD simulations were performed using commercial software (FDTD Solutions, Lumerical Inc.). Refractive index data were taken from ref. [47] after it was verified to produce similar results to the films.

## Supporting Information

Supporting Information is available from the Wiley Online Library or from the author.

## Acknowledgements

This work was funded by the Israeli Ministry of Science and Technology. A.K. was supported by a fellowship from the Center for Nanoscience and Nanotechnology of the Hebrew University. C.F. was supported by the Carlsberg Foundation as an Internationalization Fellow. The authors thank Prof. Lioz Etgar and Bat-El Cohen for the guidance on preparing perovskite films, Avner Shaltiel for the design of the imprint machine, and the staff of the Center for Nanoscience and Nanotechnology of the Hebrew University for their everlasting support.

## Conflict of Interest

The authors declare no conflict of interest.

## Author Contributions

A.K. prepared the perovskite solutions, soft lithography molds, imprinting process, and performed the SEM imaging. N.M. prepared the silicon master mold. A.K., C.F., and S.R.K.C.I. performed the optical measurements and AFM measurements. A.K. and S.R.K.C.I. performed the FDTD simulations. U.L. proposed the idea and supervised the project. The manuscript was written with contributions of all authors. All authors have given approval to the final version of the manuscript.

## Keywords

metasurfaces, nanopatterning, nanophotonics, perovskites, soft lithography

Received: September 19, 2020

Published online:

- [1] A. S. Berestennikov, P. M. Voroshilov, S. V. Makarov, Y. S. Kivshar, *Appl. Phys. Rev.* **2019**, *6*, 031307.
- [2] B. Gholipour, G. Adamo, D. Cortecchia, H. N. S. Krishnamoorthy, M. D. Birowosuto, N. I. Zheludev, C. Soci, *Adv. Mater.* **2017**, *29*, 1604268.
- [3] R. A. Bone, D. W. Lee, J. M. Norman, *Appl. Opt.* **1985**, *24*, 1408.
- [4] T. C. Vogelmann, J. F. Bornman, D. J. Yates, *Physiol. Plant.* **1996**, *98*, 43.
- [5] G. Martin, D. A. Myres, T. C. Vogelmann, *J. Exp. Bot.* **1991**, *42*, 581.
- [6] T. C. Vogelmann, *Annu. Rev. Plant Physiol. Plant Mol. Biol.* **1993**, *44*, 231.
- [7] A. Y. Zhizhchenko, P. Tonkaev, D. Gets, A. Larin, D. Zuev, S. Starikov, E. V. Pustovalov, A. M. Zakharenko, S. A. Kulnich, S. Juodkasis, A. A. Kuchmizhak, S. V. Makarov, *Small* **2020**, *16*, 2000410.
- [8] Y. Gao, C. Huang, C. Hao, S. Sun, L. Zhang, C. Zhang, Z. Duan, K. Wang, Z. Jin, N. Zhang, A. V. Kildishev, C.-W. Qiu, Q. Song, S. Xiao, *ACS Nano* **2018**, *12*, 8847.
- [9] C. Zhang, S. Xiao, Y. Wang, Y. Gao, Y. Fan, C. Huang, N. Zhang, W. Yang, Q. Song, *Laser Photonics Rev.* **2019**, *13*, 1900079.
- [10] J. Harwell, J. Burch, A. Fikouras, M. C. Gather, A. Di Falco, I. D. W. Samuel, *ACS Nano* **2019**, *13*, 3823.
- [11] J. Wu, J. Chen, Y. Zhang, Z. Xu, L. Zhao, T. Liu, D. Luo, W. Yang, K. Chen, Q. Hu, F. Ye, P. Wu, R. Zhu, Q. Gong, *Nano Lett.* **2017**, *17*, 3563.
- [12] M. T. Hörantner, W. Zhang, M. Saliba, K. Wojciechowski, H. J. Snaith, *Energy Environ. Sci.* **2015**, *8*, 2041.
- [13] S. V. Makarov, V. Milichko, E. V. Ushakova, M. Omelyanovich, A. Cerdan Pasaran, R. Haroldson, B. Balachandran, H. Wang, W. Hu, Y. S. Kivshar, A. A. Zakhidov, *ACS Photonics* **2017**, *4*, 728.
- [14] O. Bar-On, P. Brenner, U. Lemmer, J. Scheuer, *Adv. Mater. Technol.* **2018**, *3*, 1800212.
- [15] H. Wang, R. Haroldson, B. Balachandran, A. Zakhidov, S. Sohal, J. Y. Chan, A. Zakhidov, W. Hu, *ACS Nano* **2016**, *10*, 10921.
- [16] B. Kwon, J. H. Kim, *J. Nanosci.* **2016**, *2016*, 6571297.
- [17] J. A. Rogers, H. H. Lee, *Unconventional Nanopatterning Techniques and Applications*, Wiley, New York **2008**.
- [18] S. Park, S. W. Heo, W. Lee, D. Inoue, Z. Jiang, K. Yu, H. Jinno, D. Hashizume, M. Sekino, T. Yokota, K. Fukuda, K. Tajima, T. Someya, *Nature* **2018**, *561*, 516.
- [19] J. Mao, W. E. I. Sha, H. Zhang, X. Ren, J. Zhuang, V. A. L. Roy, K. S. Wong, W. C. H. Choy, *Adv. Funct. Mater.* **2017**, *27*, 1606525.

- [20] M. E. Kamminga, H.-H. Fang, M. A. Loi, G. H. ten Brink, G. R. Blake, T. T. M. Palstra, J. E. ten Elshof, *ACS Appl. Mater. Interfaces* **2018**, *10*, 12878.
- [21] B. Jeong, I. Hwang, S. H. Cho, E. H. Kim, S. Cha, J. Lee, H. S. Kang, S. M. Cho, H. Choi, C. Park, *ACS Nano* **2016**, *10*, 9026.
- [22] D. H. Chun, Y. J. Choi, Y. In, J. K. Nam, Y. J. Choi, S. Yun, W. Kim, D. Choi, D. Kim, H. Shin, J. H. Cho, J. H. Park, *ACS Nano* **2018**, *12*, 8564.
- [23] Y. Wang, P. Wang, X. Zhou, C. Li, H. Li, X. Hu, F. Li, X. Liu, M. Li, Y. Song, *Adv. Energy Mater.* **2018**, *8*, 1702960.
- [24] K. Deng, Z. Liu, M. Wang, L. Li, *Adv. Funct. Mater.* **2019**, *29*, 1900830.
- [25] T. W. Odom, J. C. Love, D. B. Wolfe, K. E. Paul, G. M. Whitesides, *Langmuir* **2002**, *18*, 5314.
- [26] H. Schmid, B. Michel, *Macromolecules* **2000**, *33*, 3042.
- [27] J. Jurin, *Philos. Trans. R. Soc. London* **1719**, *30*, 739.
- [28] Y. S. Kim, K. Y. Suh, H. H. Lee, *Appl. Phys. Lett.* **2001**, *79*, 2285.
- [29] S. Brittman, S. Z. Oener, K. Guo, H. Āboliņš, A. F. Koenderink, E. C. Garnett, *J. Mater. Chem. C* **2017**, *5*, 8301.
- [30] M. Xiao, F. Huang, W. Huang, Y. Dkhissi, Y. Zhu, J. Etheridge, A. Gray-Weale, U. Bach, Y.-B. Cheng, L. Spiccia, *Angew. Chem., Int. Ed.* **2014**, *53*, 9898.
- [31] E. M. Purcell, *Phys. Rev.* **1946**, *69*, 37.
- [32] M. Pelton, *Nat. Photonics* **2015**, *9*, 427.
- [33] G. W. Burr, S. Diziain, M.-P. Bernal, *Opt. Express* **2008**, *16*, 6302.
- [34] L. M. Pazos-Outón, M. Szumilo, R. Lamboll, J. M. Richter, M. Crespo-Quesada, M. Abdi-Jalebi, H. J. Beeson, M. Vrućinić, M. Alsari, H. J. Snaith, B. Ehrler, R. H. Friend, F. Deschler, *Science* **2016**, *351*, 1430.
- [35] M. Mirsafaei, A. H. Fallahpour, P. Lugli, H.-G. Rubahn, J. Adam, M. Madsen, *Sci. Rep.* **2017**, *7*, 5300.
- [36] J.-F. Liao, W.-Q. Wu, Y. Jiang, D.-B. Kuang, L. Wang, *Sol. RRL* **2019**, *3*, 1800268.
- [37] R. T. Ross, *J. Chem. Phys.* **1967**, *46*, 4590.
- [38] O. D. Miller, E. Yablonovitch, S. R. Kurtz, *IEEE J. Photovoltaics* **2012**, *2*, 303.
- [39] M. A. Green, *Prog. Photovoltaics* **2012**, *20*, 472.
- [40] T. Kirchartz, F. Staub, U. Rau, *ACS Energy Lett.* **2016**, *1*, 731.
- [41] S. Nanz, R. Schmager, M. G. Abebe, C. Willig, A. Wickberg, A. Abass, G. Gomard, M. Wegener, U. W. Paetzold, C. Rockstuhl, *APL Photonics* **2019**, *4*, 076104.
- [42] Best Research-Cell Efficiencies, National Renewable Energy Laboratory, <https://www.nrel.gov/pv/assets/pdfs/best-research-cell-efficiencies.20200925.pdf> (accessed: March 2020).
- [43] N. Koo, M. Bender, U. Plachetka, A. Fuchs, T. Wahlbrink, J. Bolten, H. Kurz, *Microelectron. Eng.* **2007**, *84*, 904.
- [44] N. J. Jeon, J. H. Noh, Y. C. Kim, W. S. Yang, S. Ryu, S. Il Seok, *Nat. Mater.* **2014**, *13*, 897.
- [45] J. Bar-David, N. Mazurski, U. Levy, *ACS Photonics* **2017**, *4*, 2359.
- [46] S. R. K. C. Indukuri, J. Bar-David, N. Mazurski, U. Levy, *ACS Nano* **2019**, *13*, 11770.
- [47] J. M. Ball, S. D. Stranks, M. T. Hörantner, S. Hüttner, W. Zhang, E. J. W. Crossland, I. Ramirez, M. Riede, M. B. Johnston, R. H. Friend, H. J. Snaith, *Energy Environ. Sci.* **2015**, *8*, 602.